DPNU-94-32
KEK Preprint 94-101
TIT-HPE-94-07
TUAT-HEP 94-3
INS-REP-1062
NWU-HEP 94-03
OCU-HEP 94-5
KOBE-HEP 94-04
PU-94-684

Measurement of the forward-backward asymmetries for charm- and bottom-quark pair productions at $\langle\sqrt{s}\rangle$=58GeV with electron tagging *

TOPAZ Collaboration

E.Nakano[a], † R.Enomoto[b], M.Iwasaki[c], K.Abe[a], T.Abe[a], I.Adachi[b], K.Adachi[c], M.Aoki[d], M.Aoki[a], S.Awa[c], R.Belusevic[b], K.Emi[c], H.Fujii[b], K.Fujii[b],T.Fujii[j], J.Fujimoto[b], K.Fujita[g], N.Fujiwara[c], H.Hayashii[c], B.Howell[h], N.Iida[b], H.Ikeda[b], R.Itoh[b], Y.Inoue[g], H.Iwasaki[b], K.Kaneyuki[d], R.Kajikawa[a], S.Kato[i], S.Kawabata[b], H.Kichimi[b], M.Kobayashi[b], D.Koltick[h], I.Levine[h], S.Minami[d], K.Miyabayashi[a], A.Miyamoto[b], K.Muramatsu[c], K.Nagai[j], K.Nakabayashi[a], O.Nitoh[e], S.Noguchi[c], A.Ochi[d], F.Ochiai[k], N.Ohishi[a], Y.Ohnishi[a], Y.Ohshima[d], H.Okuno[i], T.Okusawa[g],T.Shinohara[c], A.Sugiyama[a], S.Suzuki[a], S.Suzuki[d], K.Takahashi[c], T.Takahashi[g], T.Tanimori[d], T.Tauchi[b], Y.Teramoto[g], N.Toomi[c], T.Tsukamoto[b], O.Tsumura[c], S.Uno[b], T.Watanabe[d], Y.Watanabe[d], A.Yamaguchi[c], A.Yamamoto[b],and M.Yamauchi[b]

*to be published in Physics Letters B
†internet address;NAKANOE@KEKVAX.KEK.JP

(a) Department of Physics, Nagoya University, Nagoya 464, Japan
(b) KEK, National Laboratory for High Energy Physics, Ibaraki-ken 305, Japan
(c) Department of Physics, Nara Women's University, Nara 630, Japan
(d) Department of Physics, Tokyo Institute of Technology, Tokyo 152, Japan
(e) Department of Applied Physics, Tokyo Univ. of Agriculture and Technology, Tokyo 184, Japan
(f) Department of Physics, University of Tokyo, Tokyo 113, Japan
(g) Department of Physics, Osaka City University, Osaka 558, Japan
(h) Department of Physics, Purdue University, West Lafayette, IN 47907, USA
(i) Institute for Nuclear Study, University of Tokyo, Tanashi, Tokyo 188, Japan
(j) The Graduate School of Science and Technology, Kobe University, Kobe 657, Japan
(k) Faculty of Liberal Arts, Tezukayama University, Nara 631, Japan

Abstract

We have measured, with electron tagging, the forward-backward asymmetries of charm- and bottom-quark pair productions at $\langle\sqrt{s}\rangle$=58.01GeV, based on 23,783 hadronic events selected from a data sample of 197pb^{-1} taken with the TOPAZ detector at TRISTAN. The measured forward-backward asymmetries are $A^c_{FB} = -0.49\pm0.20(stat.)\pm0.08(sys.)$ and $A^b_{FB} = -0.64\pm0.35(stat.)\pm0.13(sys.)$, which are consistent with the standard model predictions.

1 Introduction

The differential cross section for fermion pair productions, $e^+e^- \to f\bar{f}$, can be written in the following form in the massless limit:

$$\frac{d\sigma_f}{d\cos\theta} = \frac{3}{8}\sigma_{f\bar{f}}(1+\cos^2\theta + \frac{8}{3}A_{FB}^f\cos\theta),$$

where $\sigma_{f\bar{f}}$ and A_{FB}^f are the total cross section and the forward-backward charge asymmetry, respectively, while θ is the polar-angle of the final-state fermion f with respect to the direction of the initial-state electron.

In the standard model[1], A_{FB}^f is given by

$$A_{FB}^f = \frac{3}{4}\cdot\frac{-2Q_f a_e a_f \Re(\chi) + 4a_e v_e a_f v_f |\chi|^2}{Q_f^2 - 2Q_f v_e v_f \Re(\chi) + (v_e^2+a_e^2)(v_f^2+a_f^2)|\chi|^2}$$

with

$$\chi = \frac{s}{16\sin^2\theta_W\cos^2\theta_W(s - M_{Z^0}^2 + iM_{Z^0}\Gamma_{Z^0}^0)},$$

where $v_e(v_f)$ and $a_e(a_f)$ are the vector and axial-vector coupling constants of the electron (final-state fermion) to the Z^0 boson, Q_f is the charge of the final-state fermion, and M_{Z^0} and $\Gamma_{Z^0}^0$ are the mass and the total width of the Z^0 boson, respectively. The standard model predicts

$$v_f = 2(I_3^f - 2Q_f\sin^2\theta_W)$$

and

$$a_f = 2I_3^f,$$

where I_3^f is the third component of the weak isospin of the fermion (f) and θ_W is the Weinberg angle.

The above formula tells us that A_{FB}^f attains to its maximum in the TRISTAN energy region and that its measurement there is sensitive to a_f and therefore to the structure of

the multiplet to which the fermion belongs. The measurement of the forward-backward charge asymmetry thus provides a good test of the standard model. The predicted asymmetries for charm- and bottom-quark pair productions are

$$A_{FB}^c = -0.47,$$
$$A_{FB}^b = -0.59$$

at $\sqrt{s}$=58.01GeV for $M_{Z^0} = 91.1888\text{GeV/c}^2$, $\Gamma_{Z^0} = 2.4974\text{GeV}$, and $\sin^2\theta_W = 0.2321$ [2]. The A_{FB}^b is, however, reduced by the B-$\bar{B}$ mixing, whose probability χ is given by $\chi = R_d\chi_d + R_s\chi_s$, where R_i, and χ_i are the fraction and the mixing probability of B_d or B_s, respectively. Their measured values[3] are

$$\chi_d = 0.16, R_d = \frac{1.0}{2.3}$$

and

$$\chi_s = 0.53, R_s = \frac{0.3}{2.3},$$

so that the expected A_{FB}^b value becomes -0.43.

In this energy region, only the data from the TRISTAN experiments are available and the TRISTAN average values of A_{FB}^c[4, 5, 6] and A_{FB}^b[7, 8, 9, 5, 10] have been

$$A_{FB}^c = -0.56 \pm 0.09,$$
$$A_{FB}^b = -0.59 \pm 0.09.$$

The A_{FB}^c is consistent with the standard model predictions and the A_{FB}^b is slightly deviated from it.

The TRISTAN data include our previous measurement[4] of the forward-backward charge asymmetry for the charm-quark pair production through both exclusive and inclusive reconstructions of $D^{*\pm} \to \pi^\pm D^0$: $A_{FB}^c = -0.49^{+0.14}_{-0.13}(stat.) \pm 0.06(sys.)$, consistent with the standard model prediction.

In order to improve the statistical accuracy, we have carried out another measurements using electron tagging to be described in this paper. It should be noted that this measurement is completely independent of the above D^* analysis and that, in our energy region, there is only one previous A_{FB}^c measurement reported, which are used lepton tagging at this $\sqrt{s}$ [5].

2 The TOPAZ detector

The main components of the TOPAZ detector[11] include a time projection chamber (TPC) and a barrel lead-glass calorimeter (BCL) which were essential to electron identification.

Combining the dE/dx information from the TPC and the E/P information from the BCL, we were able to select electrons in hadronic final states with high purity and high efficiency over a broad momentum range.

Instead of getting into details of these detectors, we summarize their performance here. The momentum resolution of the TPC has been measured to be

$$\frac{\sigma_{P_t}}{P_t} = \sqrt{1.0 + 1.0 P_t^2 (GeV/c)^2} \ \%$$

through $e^+e^- \to \mu^+\mu^-$ and cosmic $\mu^\pm$ events[11], while its dE/dx resolution was determined to be 4.6% by a study of minimum ionizing pions. The energy resolution of the BCL can, on the other hand, be expressed as

$$\frac{\sigma_E}{E} = \sqrt{\left(\frac{8.0}{\sqrt{E(GeV)}}\right)^2 + (1.5)^2} \ \%.$$

3 Analysis

3.1 Electron selection

This analysis is based on 23,783 hadronic events. The selection method was described in Ref[12]. This data sample corresponded to an integrated luminosity of 197pb^{-1} and was taken at an averaged center-of-mass energy ($\sqrt{s}$)=58.01GeV.

In search of electron track candidates, we first selected good charged tracks from the hadronic events, using the following selection criteria defining a good track.

1. The closest approach to the interaction point (R) had to be less than 1.0cm in the X-Y plane (perpendicular to the beam axis) and that in the Z direction (Z) to be less than 4.0cm.

2. the absolute value of the cosine of the polar angle had to be between 0.02 and 0.83,

3. the transverse momentum (P_t) with respect to the beam axis had to be greater than 0.15GeV/c,

4. the number of degrees of freedom (N.D.F.) in the track fitting had to be greater than 3, and

5. there had to be more than 30 hit wires for dE/dx calculation (65%-truncated mean) out of 114 wires maximum.

Each good track was extrapolated to the BCL to look for its corresponding BCL cluster and to test E/P. The clustering of the energy deposits in the BCL was carried out iteratively by merging a counter to its neighboring counter if its energy was smaller than that of the neighboring counter. For each of so formed clusters, we calculated its

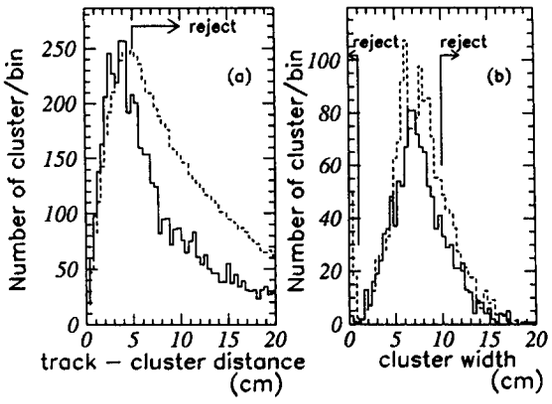

Figure 1: (a) The distribution of the minimum distance between the extrapolated track position on the BCL and the cluster position. (b) The distribution of the cluster width of a shower with respect to the track-extrapolated position. The solid and dashed histograms are for the electron-enhanced sample defined in the text and for all tracks, respectively.

energy as the sum over counters and its position as the energy-weighted mean of the counter positions.

Comparing the extrapolated track position and the BCL cluster positions, we looked for the cluster that is the closest to the track. The closest distances between tracks and clusters are histogrammed in Fig.1-(a) for all tracks (dashed) and for an electron-enhanced sample (solid) selected by requiring 0.75<E/P<1.25 and 5.5<dE/dx<7.5(keV/cm). We accepted those tracks which had a distance less than 5.0 cm.

We also calculated the energy-weighted r.m.s. of counter positions in the cluster (cluster width) with respect to the matched track position, whose distribution is shown in Fig.1-(b). The selected tracks were further required to have a cluster width between 1.0 and 10.0cm.

Since background tracks were predominantly in the low-momentum region, we imposed an additional momentum cut $P > 0.8$GeV/c.

Finally, the dE/dx information from the TPC was used to complete our electron selection: the χ^2 for electron hypothesis (χ^2_e) had to be $\chi^2_e < 3.0$ (N.D.F. = 1). The tracks rejected by this cut (dE/dx-rejected hadrons) are to be used in the background estimation.

3.2 Rejection of e^+e^- pair background

We rejected electrons apparently coming from γ conversions or Dalitz decays as follows. Secondary vertices were reconstructed for all unlike-sign pairs of the TPC tracks. When the two tracks in a pair did not intersect in the X-Y plane, we required the pair to have a distance at the closest point less than 4.0cm in the X-Y plane, and 2.0cm in the Z direction. The pair also had to have a deflection angle in the X-Y plane less than 5.0 degrees between its momentum vector and the flight direction from the interaction point. If the invariant mass of the pair was less than 50MeV/c^2, the tracks were rejected.

When the tracks intersected in the X-Y plane, we selected from the two intersections the one which gave the smaller deflection angle as the secondary vertex. We then required the pair to have a distance less than 2.0cm in the Z direction and to have a deflection angle less than 5.0 degrees. If the invariant mass was less than 200MeV/c^2, the tracks were rejected.

In this way, most of the electrons coming from γ conversions or Dalitz decays were removed. Nevertheless, there still remained a significant number of electrons from γ conversions or Dalitz decays, which were estimated through Monte-Carlo simulation[13]: the Monte-Carlo simulation gave us the ratio of the number of all the reconstructed conversion tracks to that of the remaining tracks.

Using this ratio, we estimated the number of remaining pair-conversion tracks from the actual number of all the reconstructed pairs in the experimental data on a bin by bin basis and subtracted them from the electron candidates. By doing this, we can reduce the systematic errors due to the error of the material thickness in the detector simulation program. The remaining electrons from γ conversions or Dalitz decays estimated through the Monte-Carlo simulation are 311.7 ± 17.7 events. The E/P distribution for these electron candidates is shown in Fig.2.

3.3 Hadron background

The hadron background was estimated using the dE/dx-rejected hadrons in the experimental data and is shown in Fig.2 as the dashed histogram, whose normalization factor was calculated so as to equalize the entries in the side-band (E/P = 0.0 - 0.64) for the electron candidates and the background sample. The normalized background was subtracted from the electron candidates and the remaining electrons in the region 0.72<E/P<2.00 were counted. This method had been checked out through the Monte-Carlo simulation.

The estimated number of electrons from primary charm, b-to-c cascade, and direct bottom decays are 151.5 ± 12.3, 66.5 ± 8.2, and 131.9 ± 11.5 events, where the selection efficiencies of 10.4%, 11.3%, and 24.1%, respectively.

3.4 Charm- and bottom-quark sample

We calculated the transverse momentum (P_T) of each electron candidate track with respect to the axis of jets reconstructed using the invariant-mass algorithm [4]. For the jet reconstruction, we used charged tracks with momenta greater than 0.2GeV/c and all of the neutral clusters, which were clusters with a distance to the closest track greater

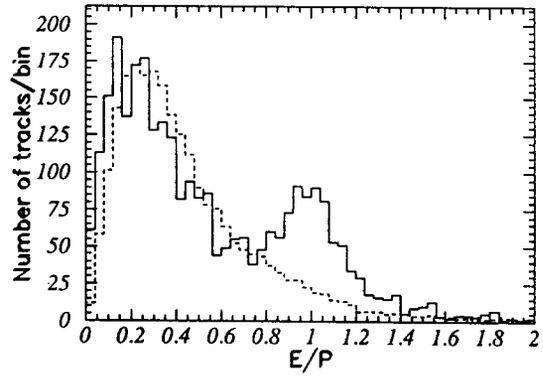

Figure 2: The E/P distribution of the selected electron samples. The solid histogram shows the experimental data. The dashed histogram is for the estimated background by dE/dx-rejected hadrons.

than 5.0 cm.

We studied the angular resolution of the jet axis with respect to the primary quark direction through the Monte-Carlo simulation. Since the resolution of the thrust axis was about 9 degrees, while that of the reconstructed jets as above was about 6 degrees, we used the reconstructed jets as the primary quark directions.

The P_T of an electron from a charm-quark is expected to be lower than that of a bottom-quark in general. To enhance charm or bottom contents, therefore, we divided the sample at $P_T = 0.8$GeV/c into two classes: low-P_T (charm-enhanced) and high-P_T (bottom-enhanced) samples.

3.5 Monte Carlo simulation

We generated Monte-Carlo events using the JETSET6.3 generator [13] with $M_{Z^0} = 91.173\text{GeV/c}^2, \Gamma_{Z^0} = 2.487\text{GeV}$, and $\sin^2\theta_W = 0.2325$[3]. For light quark events, its

parameters were tuned by a multi-parameter fit of hadronic event shapes[12]. For heavy quark events, we adjusted the parameters for fragmentation function, so as to match other experiments[5], to be a=0.8 and b=0.2. The B-$\bar{B}$ mixing effect is included in our Monte-Carlo simulation. Using this Monte-Carlo simulation, we estimated the acceptance and radiative correction factors to be used later in the following subsection.

3.6 Fitting procedure

Figs.3-(a) and -(b) show the momentum and the P_T distributions of electrons, respectively. The $-Q\cos\theta$ distributions of the high-P_T and the low-P_T electrons are shown in Figs.4-(a) and -(b), respectively, where Q is the charge of the electron and θ is the polar angle of the jet axis with respect to the electron beam axis. The points with error bars in the figures are experimental data, while the histograms are the best-fit results obtained by fitting Fig.3-(a), Figs.4-(a), and -(b) simultaneously. The used fit function to the $-Q\cos\theta$ distribution is

$$\begin{aligned} N_i^{e^\pm} &= N_{q\bar{q}}^{exp}\frac{\sigma_{c\bar{c}}}{\sigma_{q\bar{q}}}\cdot 2Br(c\to e)F(-A_{FB}^c)_i\cdot C_i^{pc} \\ &+ N_{q\bar{q}}^{exp}\frac{\sigma_{b\bar{b}}}{\sigma_{q\bar{q}}}\cdot 2Br(b\to e)F(A_{FB}^b)_i\cdot C_i^{pb} \\ &+ N_{q\bar{q}}^{exp}\frac{\sigma_{b\bar{b}}}{\sigma_{q\bar{q}}}\cdot 2Br(c\to e)(1+x)F(-\frac{1-x}{1+x}A_{FB}^b)_i\cdot C_i^{ca} \end{aligned}$$

with $x\equiv Br(b\to c\bar{c}s)$ set to be 16%[14], where, $N_{q\bar{q}}^{exp}$ is the number of hadronic events, and $F(A_{FB}^j)_i$ are integrals of the following formula over i-th $\cos\theta$ bin;

$$\frac{3}{8}(1+\cos^2\theta+\frac{8}{3}A_{FB}^j\cos\theta).$$

C_i^{pc}, C_i^{pb}, and C_i^{ca} are the Monte-Carlo-determined correction factors for the i-th bin of electrons from prompt charm, prompt bottom, and b-to-c cascade decays, respectively, which were described in the previous subsection and they are listed in Table 1.

$\cos\theta$ region		prompt charm C_i^{pc}		prompt bottom C_i^{pb}		b-to-c cascade C_i^{ca}	
		low-P_T	high-P_T	low-P_T	high-P_T	low-P_T	high-P_T
-0.77	-0.6	0.0967	0.0185	0.1134	0.1220	0.1006	0.0216
-0.6	-0.4	0.1640	0.0164	0.1156	0.1748	0.0971	0.0470
-0.4	-0.2	0.1319	0.0234	0.1275	0.1949	0.1552	0.0274
-0.2	0.0	0.1430	0.0224	0.1182	0.1785	0.1358	0.0340
0.0	0.2	0.1212	0.0177	0.1398	0.1761	0.1147	0.0247
0.2	0.4	0.1373	0.0211	0.1196	0.1865	0.1063	0.0399
0.4	0.6	0.1308	0.0160	0.1096	0.1437	0.1258	0.0362
0.6	0.77	0.0830	0.0120	0.0682	0.1607	0.0696	0.0253

Table 1: List of correction factors.

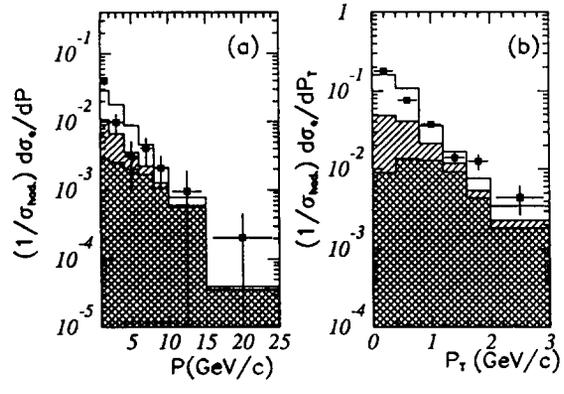

Figure 3: (a) The momentum distribution of $e^\pm$'s. (b) The P_T distribution of $e^\pm$'s. The points are background-subtracted data. The open, hatched, and double-hatched histograms are the best-fit results for the contributions from $c\to e^+X$, $b\to c\to e^+X$, and $b\to e^-X$, respectively.

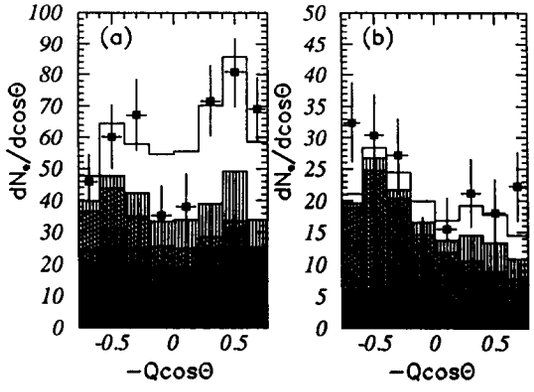

Figure 4: The -Qcos θ distributions of $e^{\pm}$'s (a)in the low-P_T region (P_T < 0.8GeV/c) and (b)in the high-P_T region (P_T > 0.8GeV/c). The points are experimental data. The open, hatched, double-hatched, triple-hatched, and filled histograms are the best-fit results for the contributions from $c \to e^-X, \bar{b} \to \bar{c} \to e^-X, \bar{c} \to e^-X$, γ conversion, and Dalitz decay, respectively.

The fit determined the branching fractions of $c \to e$ and $b \to e$ to be

$$Br(c \to e) = 0.131 \pm 0.015$$
$$Br(b \to e) = 0.109 \pm 0.025$$

and A^c_{FB} and A^b_{FB} to be

$$A^c_{FB} = -0.49 \pm 0.20$$
$$A^b_{FB} = -0.64 \pm 0.35.$$

3.7 Systematic errors

We checked various systematic-error sources. The estimated systematic errors are summarized in Table 2 and the varied parameter values used for the estimation are listed in Table 3. The dependence on the selection of good tracks was checked by changing

error source	$\frac{\Delta Br(c\to e)}{Br(c\to e)}$	$\frac{\Delta A^c_{FB}}{A^c_{FB}}$	$\frac{\Delta Br(b\to e)}{Br(b\to e)}$	$\frac{\Delta A^b_{FB}}{A^b_{FB}}$
track selection	7.4%	3.3%	6.4%	17.7%
dE/dx	1.0%	7.5%	1.3%	3.2%
cluster selection	5.7%	6.8%	10.5%	0.6%
background	2.2%	8.2%	1.7%	6.7%
γ and Dalitz rejection	1.5%	1.0%	1.6%	1.5%
P_T cut	3.0%	8.3%	8.1%	7.2%
total	10.2%	15.8%	14.9%	20.6%

Table 2: Summary of systematic errors.

the cut values on R, Z, P_t, and momentum (P). The dE/dx dependence was tested by changing the χ^2_e cut. The error caused by the shower shape parameters was estimated by changing the distance cut and the cluster width cut. We checked the effect of the background estimation by changing the region for background normalization and electron counting: the first set used 0.0<E/P<0.64 and 0.72<E/P<2.00 for normalization and counting, respectively, while the second one used 0.40<E/P<0.60 and 1.6<E/P<2.00 for normalization and 0.72<E/P<1.28 for counting. The systematic error due to the estimation of the γ conversions and Dalitz decays was checked by changing the cuts for the γ conversion and Dalitz decay rejection. The QCD correction was estimated by comparing the JETSET 6.3 P.S. and JETSET 6.3 $q\bar{q}$ options to be -0.02 and -0.01 for A^c_{FB} and A^b_{FB}, respectively. Since they were small, we neglected them. The errors from the P_T cut is also given in Table 2. The errors due to uncertainty of B-$\bar{B}$ mixing were also checked and they were negligibly small($\sim$ 0.2%). The overall systematic errors were obtained by adding them in quadrature.

error source	parameter	nominal value	varied value
track selection	R	1.0cm	1.2cm
	Z	4.0cm	3.0cm
	P_t	0.15GeV/c	0.20GeV/c
	P	0.8GeV/c	1.0GeV/c
dE/dx	χ^2_e	3.0	2.7
cluster selection	distance	5.0cm	7.5cm
	width	1.0 - 10.0cm	2.0 - 12.5cm
γ and Dalitz rejection	X-Y distance	4.0cm	5.0cm
	Z distance	2.0cm	2.5cm
	deflection angle	5 degrees	7 degrees
P_T cut		0.80GeV/c	0.75GeV/c
B-$\bar{B}$ mixing	χ	0.139	0.0

Table 3: Summary of varied parameter values.

3.8 Results and discussion

Our results are

$$Br(c \to e) = 0.131 \pm 0.015(stat.) \pm 0.013(sys.)$$
$$Br(b \to e) = 0.109 \pm 0.025(stat.) \pm 0.016(sys.)$$
$$A^c_{FB} = -0.49 \pm 0.20(stat.) \pm 0.08(sys.)$$
$$A^b_{FB} = -0.64 \pm 0.35(stat.) \pm 0.13(sys.).$$

The branching fractions are consistent with the previous measurements, and the forward-backward asymmetries are consistent with the standard model predictions as well as our previous measurements [4, 8, 9]. The obtained forward-backward asymmetry for charm-quark pair production is plotted in Fig. 5 together with other experimental data [2, 4, 5, 6, 15].

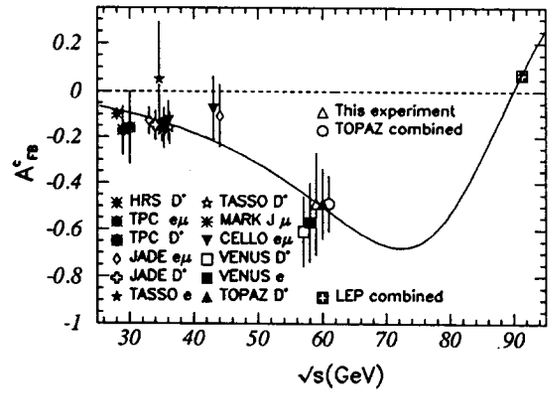

Figure 5: Our A^c_{FB} measurements together with other experimental data shown as a function of $\sqrt{s}$.

The combined result with our previous D^* analysis is

$$A^c_{FB} = -0.49 \pm 0.12,$$

from which we obtain the charm-quark's axial-vector coupling constant(a^c_v) to the Z^0 boson to be $a^c_v = 1.07^{+0.42}_{-0.31}$, being consistent with the standard model.

4 Conclusion

We have measured the forward-backward asymmetries of charm- and bottom-quark pair productions via e^+e^- annihilations through an inclusive electron analysis at $\langle\sqrt{s}\rangle$=58.01GeV. The number of hadronic events used for this analysis is 23,783, corresponding to an integrated luminosity of 197pb^{-1}.

The measured forward-backward asymmetries are $A^c_{FB} = -0.49 \pm 0.20(stat.) \pm 0.08(sys.)$ and $A^b_{FB} = -0.64 \pm 0.35(stat.) \pm 0.13(sys.)$, consistent with the standard model prediction and our previous measurements. Combining the results from our

previous $D^{*\pm}$ measurement, we obtained $A_{FB}^{c} = -0.49 \pm 0.12$ and $a_v^c = 1.07^{+0.42}_{-0.31}$. The obtained branching fractions are $Br(c \to e) = 13.1 \pm 1.5(stat.) \pm 1.3(sys.)\%$ and $Br(b \to e) = 10.9 \pm 2.5(stat.) \pm 1.6(sys.)\%$, which are in good agreement with the previously measured values of $9.6 \pm 0.9\%$[16] and $10.8 \pm 0.5\%$[16, 17], respectively.

5 Acknowledgement

The authors thank Dr. M. Sakuda for discussions on the analysis. They also thank the TRISTAN accelerator staff for the successful operation of TRISTAN. The authors appreciate all of the engineers and technicians at KEK as well as the collaborating institutions: H. Inoue, N. Kimura, K. Shiino, M. Tanaka, K. Tsukada, N. Ujiie, and H. Yamaoka.

References

[1] S. Weinberg, Phys. Rev. Lett. 19 (1967) 1264;
A. Salam, in: Elementary particle theory; relativistic group and analyticity, Nobel Symp. No. 8, ed. N. Svartholm (Almqvist and Wiksells, Stockholm, 1968) p. 361;
S. L. Glashow, Nucl. Phys. 22 (1961) 1579.

[2] D. Schaile, in: 27th Intl. Conf. on High Energy Physics (Glasgow, 1994)

[3] Particle Data Group, Phys. Rev. D45, No.11, Part II (1992).

[4] E. Nakano et al., Phys. Lett. B 314 (1993) 471.

[5] K. Abe et al., Phys. Lett. B 313 (1993) 288.

[6] F. Hinode et al., Phys. Lett. B 313 (1993) 245.

[7] F. Liu et al., KEK Preprint 93-147 submitted to Phys. Rev. D

[8] A. Shimonaka et al., Phys. Lett. B 268 (1991) 457.

[9] K. Nagai et al., Phys. Lett. B 278 (1992) 506.

[10] M. Shirakata et al., Phys. Lett. B 278(1992) 499.

[11] R. Enomoto et al., Nucl. Instrum. Methods A 269 (1988) 507;
A. Imanishi et al., Nucl. Instrum. Methods A 269 (1988) 513;
T. Kamae et al., Nucl. Instrum. Methods A 252 (1986) 423;
A. Yamamoto et al., Jpn. J. Appl. Phys. Lett. 25 (1986) L440;
S. Kawabata et al., Nucl. Instrum. Methods A 270 (1988) 11;
J. Fujimoto et al., Nucl. Instrum. Methods A 256 (1987) 449;

S. Noguchi et al., Nucl. Instrum. Methods A 271 (1988) 404;
K.Fujii et al., Nucl. Instrum. Methods A 264 (1988) 297.

[12] I. Adachi et al., Phys. Lett. B 255 (1991) 613.

[13] T. Sjostrand, Comput. Phys. Commun. 39 (1986) 347;
T. Sjostrand and M. Bengtsson, Comput. Phys. Commun. 43 (1987) 367.

[14] J. Leveille, in: Proc. second Moriond Workshop (Moriond, 1982), eds. J. Tran Thanh Van and L. Montanet, P.191

[15] M. Althoff et al., Phys. Lett. B 126 (1983) 493;
W. Braunschweig et al., Z. Phys. C 44 (1989) 365;
W. Bartel et al., Phys. Lett. B 146 (1984) 121;
F. Ould-Saada et al., Z. Phys. C 44 (1989) 567;
H. Aihara et al., Phys. Rev. D 34 (1986) 1945;
M. Derrick et al., Phys. Lett. B 146 (1984) 261;
P. Baringer et al., Phys. Lett. B 206 (1988) 551;
H. Aihara et al., Z. Phys. C 27 (1985) 39;
H. Aihara et al., Phys. Rev. D 31 (1985) 2719;
M. Althoff et al., Phys. Lett. B 146 (1984) 443;
H. J. Behrend et al., Z. Phys. C 47 (1990) 333;
E. Elsen et al., Z. Phys. C 46 (1990) 349;
B. Adeva et al., Phys. Rep. 109 (1984) 131.

[16] H. Albrecht et al., Phys. Lett. B 249 (1990) 359.

[17] S. Henderson et al., Phys. Rev. D 45 (1992) 2212.